2008 IEEE International Conference on
Robotics and Automation
Pasadena, CA, USA, May 19-23, 2008

Network-Based Intelligent Space Approach for Car-Like Mobile Robots by Fuzzy Decentralized Variable Structure Control

Chih-Lyang Hwang and Li-Jui Chang
Department of Electrical Engineering, Tamkang University, Taiwan

Abstract **--- To realize trajectory tracking and obstacle avoidance, two distributed CCD (charge-coupled device) cameras are constructed to obtain the dynamic poses of the car-like mobile robots (CLMRs) and the obstacles. Based on the control authority of these two CCD cameras, a suitable reference command including desired steering angle and translation velocity for the fuzzy decentralized variable structure control (FDVSC) in the client computer is on-line planned. Due to the delay of signal transmission through an internet network and wireless local area network (WLAN), suitable sampling time of the FDVSC is determined by the Quality of Service (QoS). The proposed control can track an on-line planning reference command without the requirement of a mathematical model of the CLMR. Only the information of the upper bound of system knowledge (including the dynamics of the CLMR, the delay feature of internet network and WLAN) is required to select the suitable scaling factors and the coefficients of switching surface so that an acceptable performance is achieved.**

Index Terms: Network-based intelligent space, Car-like mobile robot, Trajectory tracking, Obstacle avoidance, Fuzzy decentralized variable structure control.

I. INTRODUCTION

Recently, distributed control applications within sensor networks are gaining a role of importance (e.g., [1]). Such network-based intelligent spaces are able to monitor remote equipments what is occurring themselves, to build their own models, to communicate with their inhabitants, and to act on the basis of decisions they make. For instance, a remotely-controlled wheelchair (or mobile robot) is designed to track a trajectory, which is often made up by a set of piecewise lines due to the constraint of architecture. It indicates that a set of piecewise straight lines is practical for a trajectory planning. Furthermore, many of the problems encountered by classic mobile robots (e.g., localization [2], large computation for on-line path planning [3], sensor-based control [4]) are solved when they are in a sensor network (or an intelligent space).

Based on this concept of "Network-Based Intelligent Space" (e.g., [1]), two distributed CCD cameras in this space are applied to provide the dynamic poses of the CLMRs and the obstacles. In this paper, only a CLMR in the two-dimension of the world coordinate is considered. The extension to multiple CLMRs will be our future work. After the image processing in the server computer, the poses of the CLMR or obstacle and the outputs of two motors in the CLMR are transmitted to the client computer so that a reference command for the FDVSC is real time planned. The control input is calculated and then transmitted to the server computer via an internet network. It is sequentially transmitted to the CLMR via a WLAN.

The controller design for the CLMR is described as follows. Because the decentralized control scheme is free from the difficulties arising from the complexity in design, debugging, data gathering, and storage requirements, it is more preferable to a mobile robot than a centralized control [5]. Recently, the so-called fuzzy decentralized variable structure control (FDVSC) provides a robust controller for the nonlinear systems [5]. The proposed control can track a reference command without the requirement of a mathematical model of the CLMR. Only the information of the system knowledge, including the upper bounds of the dynamics of the CLMR and the delay through internet network and WLAN, is needed to choose a suitable set of the scaling factors and the coefficients of sliding surface such that an acceptable performance is obtained.

To ensure the QoS, the sampling time of the overall control system must be greater than total transmission time of the closed-loop system (see, e.g., [5-7]). Under this circumstance, the stability of the closed-loop system in the face of small time-varying delay is also addressed to satisfy the requirement in the networked-based control. Finally, a sequence of experiments in a network-based intelligent space is arranged to evaluate the effectiveness of the proposed control system.

II. SYSTEM DESCRIPTION, SYSTEM ANALYSIS AND RESEARCH TASK

2.1 System Description

Fig. 1 shows the experimental setup of a CLMR in a network-based intelligent space. The overall control system includes a CLMR (including two DC motors, one microprocessor, one driver, WLAN device, and mechanism), two CCD cameras, and two personal computers connected with an internet network (i.e., the sever computer including image processing card and WLAN device; the path planning and the computation of FDVSC in the client computer). The CLMR with two wheels driving system is depicted in Fig. 2. The rear wheels are fixed parallel to the car chassis and allowed to roll or spin but are assumed to roll without slipping; two front wheels are parallel and can simultaneously turn to the right or left. For a CLMR with size and shape, its location in the 2-D Cartesian space W can be uniquely determined by the spatial position (x, y) of the base point and the orientation angle ρ with respect to the base point (see Fig. 2).

Fig. 3 shows the implementation of the CLMR. The core of the CLMR is the DSP of TMS320LF2407 from TI Co. The wireless local area network device is data

gateways between RS-232/422/486 and 802.11b WLAN interfaces supports WLAN Ad-Hoc and Infrastructure modes. It is used for data acquisition and transmission between the PC and the CLMR. The Matrox Meteor-II card is applied as an image processing card to detect the orientation and position (i.e., pose) of the CLMR.

First, three LEDs are assigned to suitable places; then, three corresponding points on image plane to represent three positions with respect to the world coordinate (i.e., $(\hat{x}_1,\hat{y}_1),(\hat{x}_2,\hat{y}_2)$, and $(\hat{x}_3,\hat{y}_3)$) in Fig. 2) are achieved. Based on the relation (1) and (2), the estimated position $\hat{x}(k),\hat{y}(k)$ and orientation $\hat{\rho}(k)$ of geometry center (i.e., pose) of the CLMR with respect to the world coordinate at the *kth* samp6ling interval are described as follows:

$$[\hat{x}(k),\hat{y}(k)]=\left[\left(2\hat{x}_1(k)+\hat{x}_2(k)+\hat{x}_3(k)\right)/4 \quad \left(2\hat{y}_1(k)+\hat{y}_2(k)+\hat{y}_3(k)\right)/4\right] \tag{1}$$

$$\hat{\rho}(k)=\tan^{-1}\left\{\left[\hat{y}_1(k)-\left(\hat{y}_2(k)+\hat{y}_3(k)\right)/2\right] /\left[\hat{x}_1(k)-\left(\hat{x}_2(k)+\hat{x}_3(k)\right)/2\right]\right\}. \tag{2}$$

2.2 System Analysis

In this subsection, the step response and the estimation of delay are employed to realize the characteristic of the proposed control system. The step responses of the front and rear wheel for a CLMR are shown in Fig. 4. It is known that the dynamics of a CLMR is nonlinear, coupled, and time-variant. The outputs of the front wheel and the rear wheel are the steering angle and the angular (or translation) velocity, respectively. Therefore, the bandwidth of the rear wheel is larger than that of the front wheel. The response of the rear wheel possesses the high frequency component; on the other hand, the response of the front wheel is smooth owing to its low-pass feature.

As one knows, the signal passing through an internet network and WLAN always has a delay feature. In general, this delay is time varying, i.e., $\tau(t)$. Based on the estimation, the delay has an upper bound of 300 *ms* (i.e., $|\tau(t)|\le\tau_u=300ms$) with the fluctuation of 50*ms* (i.e., $|\tau_u-\tau(t)|\le 50ms$).This delay feature always results in a phase lag and then the possible instability of the closed-loop system. Therefore, how to design an effective controller for the networked-based trajectory tracking and obstacle avoidance of a CLMR in an intelligent space is important.

2.3 Research Task

In this paper, the interpolation method to obtain the world coordinate (*OXY*) from the image coordinate ($O_iX_iY_i$) is used. The intelligent space includes two trapezoid areas (the 1st trapezoid has the length of upper side and lower side 244c*m*, and 144c*m*, respectively, and the depth 300c*m*; the 2nd trapezoid has the length of upper side and lower side 241c*m*, and 141c*m*, respectively, and the depth 295c*m*), an overlapped region with 24*cm*, and an offset of 12*cm* (i.e., these two trapezoids are not symmetric). The main goal of this study is to investigate the responses of the trajectory tracking and obstacle avoidance of a CLMR within networked-based intelligent space using the FDVSC. These experiments are categorized into the following four cases: (i) to track a trajectory of line segments, (ii) to track the same trajectory of part (i) with two static obstacles, (iii) to track the same trajectory of part (i) with one static and one dynamic obstacles, and (iv) to track the same trajectory of (i) without and with two static obstacles using a PID control.

III. FDVSC

Consider the following network-based CLMR:

$$A(\theta)\ddot{\theta}(t)+B(\theta,\dot{\theta})+C(\theta)+N(t)=DU_{\tau_u}(t) \tag{3}$$

where $\theta(t)\in\Re^2$ is the angle of the CLMR, $A(\theta)\in\Re^{2\times2}$ denotes the inertia matrix of positive definite for any $\theta(t)$, $B(\theta,\dot{\theta})\in\Re^2$ comprises the centrifugal, Coriolis torques, $C(\theta)\in\Re^2$ denotes the gravitational torque, $N(t)$ denotes a nonlinear time-varying uncertainty, $D\in\Re^{2\times2}$ represents a control gain, and $U_{\tau_u}(t)=U(t-\tau_u)\in\Re^2$ is the network-based control torque. It is assumed that the dynamics of (3) is unknown. However, the upper bound of function from (3) is supposed to be known.

The FDVSC includes two parallel FVSC (cf. Fig. 5), and it has two sliding surfaces shown as follows:

$$S(t)=GE(t),\ G=\begin{bmatrix}G_1 & G_2\end{bmatrix},\ E(t)=\begin{bmatrix}E_1^T(t) & E_2^T(t)\end{bmatrix}^T \tag{4}$$

where $S(t)\in\Re^2$, $G_1=diag(g_{1ii})>0, G_2=diag(g_{2ii})>0\in\Re^{2\times2}$ for $i=1,2$ are the coefficients of sliding surface, and

$$E_1(t)=\theta_r(t)-\theta(t),\ E_2(t)=\dot{E}_1(t) \tag{5}$$

where $\theta_r(t)\in\Re^2$ is a reference command which is on-line planned, $E_1(t)=\begin{bmatrix}e_1(t) & e_2(t)\end{bmatrix}^T$, and $E_2(t)=\begin{bmatrix}e_3(t) & e_4(t)\end{bmatrix}^T$. From (3) and (5), it leads to

$$\dot{E}_2(t)=\ddot{\theta}_r(t)+A^{-1}(\theta)\left\{B(\theta,\dot{\theta})+C(\theta)+N(t)-DU_{\tau_u}(t)\right\} \tag{6}$$

Then the networked-based FDVSC (NBFDVSC) is designed as follows:

$$\begin{aligned}U_{\tau_u}(t)&=G_3\overline{U}_{\tau_u}(t)=G_3\left[GE_{\tau_u}(t)+\Delta\,\mathrm{sgn}(GE_{\tau_u})\right]\\&=G_3\left[S_{\tau_u}(t)+\Delta\,\mathrm{sgn}(S_{\tau_u})\right]\end{aligned} \tag{7}$$

where $S_{\tau_u}(t)=S(t-\tau_u), E_{\tau_u}(t)=E(t-\tau_u)$, $G_3=diag(g_{3ii})>0\in\Re^{2\times2}$ is the output scaling factor, $\overline{U}_{\tau_u}(t)$ is fuzzy variable of $U_{\tau_u}(t)$, and $\Delta=diag(\delta_{ii})>0\in\Re^{2\times2}$. It is assumed that

$$g_{3ii}\ge\left\{a_M d_M\left[\left|f_i(t)\right|+\lambda_i\right]\right\}/\left(g_{2m}\delta_{ii}\right) \text{ for } i=1,2 \tag{8}$$

where $\lambda_i>0, g_{2m}=\lambda_{\min}\{G_2\}, a_M=\lambda_{\max}\{A(Y)\}, d_M=\lambda_{\max}\{D\}$, and $f_i(t)$ is the *ith* element of the following uncertainty:

$$\begin{aligned}F(t)=&G_1\left[\dot{\theta}_r(t)-\dot{\theta}(t)\right]+G_2\left\{\ddot{\theta}_r(t)+A^{-1}(\theta)\right.\\&\left.\cdot\left[B(\theta,\dot{\theta})+C(\theta)+N(t)-DG_3S_{\tau_u}(t)\right]\right\}\end{aligned} \tag{9}$$

Lemma 1: Consider a linear stable system $\dot{e}(t)+c_1e(t)=s(t)$, where $c_1>0$ and $|s(t)|\le\alpha\ \forall t$. Then $|e(t)|\le\alpha/c_1$ and $|\dot{e}(t)|\le2\alpha$ as $t\to\infty$.

Theorem 1: Applying the NBFDVSC (7) to the unknown

system (3) with the satisfaction of condition (8) gives that $\{S(t),U(t)\}$ are ultimately uniformly bounded (UUB) and a finite time (see (16)) reaches a convex set of the sliding surface:

$$\Omega=\left\{S(t)\middle\|S(t)\right\|\le c_s(\tau_u),\text{with }\operatorname{sgn}(S)\ne\operatorname{sgn}(S_{\tau_u})\right\} \quad (10)$$

where $c_s(\tau_u)$ is a positive constant dependent on τ_u, $\|S(t_0)\|>c_s(\tau_u)$, and t_0 denotes an initial time. If $\tau(t)=0$, i.e., $c_s(\tau_u)=0$, then $E(t)\to 0$ as $t\to\infty$.

Proof: Define the following Lyapunov function:

$$V(t)=S^T(t)S(t)/2>0,\text{ as } S(t)\ne 0. \quad (11)$$

Taking the time derivative of (11) gives

$$\dot V(t)=S^T(t)\dot S(t). \quad (12)$$

Substituting (5) and (6) into (12) gives

$$\begin{aligned}\dot V(t)=S^T(t)\Big\{&G_1\left[\dot\theta_r(t)-\dot\theta(t)\right]+G_2\left[\ddot\theta_r(t)\right.\\&\left.+A^{-1}(\theta)\left(B(\theta,\dot\theta)+C(\theta)+N(t)-DU_{\tau_u}(t)\right)\right]\Big\}\end{aligned} \quad (13)$$

Substituting (7) and (9) into (13) yields

$$\begin{aligned}\dot V(t)&=S^T(t)\Big\{G_1\left[\dot\theta_r(t)-\dot\theta(t)\right]\\&\quad+G_2\left[\ddot\theta_r(t)+A^{-1}(\theta)\left(B(\theta,\dot\theta)+C(\theta)+N(t)\right)\right]\Big\}\\&\quad-S^T(t)G_2A^{-1}(\theta)DG_3\left[S_{\tau_u}(t)+\Delta\operatorname{sgn}(S_{\tau_u})\right]\\&=S^T(t)F(t)-S^T(t)G_2A^{-1}(\theta)DG_3\Delta\operatorname{sgn}(S)\\&\quad-S^T(t)G_2A^{-1}(\theta)DG_3\Delta\left[\operatorname{sgn}(S_{\tau_u})-\operatorname{sgn}(S)\right].\end{aligned} \quad (14)$$

If the sliding surface is outside of the convex set Ω, i.e., $\|S(t)\|>c_s(\tau_u)$, then $\operatorname{sgn}(S)=\operatorname{sgn}(S_{\tau_u})$. Substituting this fact into (14) and using the result $G_2A^{-1}(\theta)D>0$, yields

$$\begin{aligned}\dot V(t)&\le\left\|S(t)\right\|\textstyle\sum_{i=1}^{2}\left\{\left|f_i(t)\right|-g_{2m}g_{3ii}\delta_{ii}/(a_Md_M)\right\}\\&=\left\|S(t)\right\|\textstyle\sum_{i=1}^{2}\lambda_i\le-\lambda\left\|S(t)\right\|=-\lambda\sqrt{2V(t)}\end{aligned} \quad (15)$$

where $\lambda=\min_{1\le i\le 2}(\lambda_i)$. Then, the solution of the inequality (15) for the initial time t_0 and the initial value $S(t_0)$ is expressed as follows:

$$t-t_0\le\left[\left\|S(t_0)\right\|-c_s\right]/\lambda \quad (16)$$

where t denotes the time operating point hits the boundary of the convex set of the sliding surface (10), and $t-t_0$ denotes the finite time to approach the convex set. Once the operating point reaches the convex set, the tracking error is bounded. From (4) and (7), $\{S(t),U(t)\}$ are then UUB. Based on *Lemma 1*, $|e_i(t)|\le c_s(\tau_u)/(g_{1ii}/g_{2ii})$ and $|\dot e_i(t)|\le 2c_s(\tau_u)$, i=1, 2 as $t\to\infty$. If $\tau(t)=0$, then $c_s(\tau_u)=0$ and the asymptotical tracking is obtained.

Q.E.D.

Remark 1: The last term of (14) cannot be included into the uncertainty (9) because it contains the signal (i.e., Δ) to deal with the uncertainty. If the operating point is outside of the convex set (10) and the inequality (8) is not satisfied, a larger convex set of sliding surface as compared with (10) can exist such that the inequality (8) is satisfied, a finite time reaches this convex set, and then the sequences $\{S(t),U(t)\}$ are UUB. In fact, an upper bound of τ_u must exist such that $c_s(\tau_u)$ is bounded.

Remark 2: From (13), it is assumed that $\dot s_i(t)$ increases as $u_i(t)=g_{3ii}\bar u_i(t)$ decreases, and if $s_i(t)>0$ then increasing $u_i(t)$ will result in decreasing $s_i(t)\dot s_i(t)$ and if $s_i(t)<0$ then decreasing $u_i(t)$ will result in decreasing $s_i(t)\dot s_i(t)$. Hence, the control input $u_i(t)$ is designed so as to satisfy the inequality $s_i(t)\dot s_i(t)<0$.

Remark 3: In the beginning, the fuzzy variable is quantized into the following seven qualitative fuzzy variables: (i) Positive Big (PB), (ii) Positive Medium (PM), (iii) Positive Small (PS), (iv) Zero (ZE), (v) Negative Small (NS), (vi) Negative Medium (NM), and (vii) Negative Big (NB). The inputs of fuzzy variable are defined as follows: $\bar s_i(t)=g_{sii}s_i(t)$ and $\dot{\bar s}_i(t)=g_{\dot sii}\dot s_i(t)$, where $G_s=diag\{g_{s11},g_{s22}\}$ and $G_{\dot s}=diag\{g_{\dot s11},g_{\dot s22}\}$ are applied to normalize the values $\bar s_i(t)$ and $\dot{\bar s}_i(t)$ into the interval $[-1,1]$. The triangular type in Fig. 6 is used in this application. The linguistic rule of the *ith* FDVSC is shown in Table 1 by which the center of gravity method is employed to form a look-up table that directly relates the inputs $\bar s_i(t)$ and $\dot{\bar s}_i(t)$ with the output $\bar u_i(t)$. Based on the system stability (8), the output scaling factor G_3 is chosen. Hence, the real control input $U(t)=G_3\bar U(t)$ is obtained to drive the two motors.

IV. EXPERIMENTS

4.1 Experimental Preliminaries

A. Pose estimation

Based on our experiments, the maximum estimation error is about 2*cm*, which is acceptable and merely occurs in the periphery of the trapezoid. While the CLMR is in the left trapezoid area, the pose of the CLMR or the position of (dynamic) obstacle is estimated by CCD1. After trajectory planning, the reference command for the CLMR is sent by a WLAN. Similarly, as the CLMR is in the right trapezoid area, the pose of the CLMR or the position of obstacle is estimated by CCD2; the planned reference command is also sent by the same WLAN. However, when the CLMR is inside the overlap region, two CCD cameras can grab the image and the pose of the CLMR or obstacle is estimated either by CCD1 or CCD2.

B. Tracking mode

Tracking mode of this paper includes two types: (i) approach mode, (ii) fine tune mode. The purpose of approach mode is to drive the CLMR in the neighborhood of trajectory. Then, the fine tune mode is employed to force the CLMR on the trajectory as near as possible. The content of large circle with dash-dotted line of Fig. 7 indicates the concept of fine tune mode. After the CLMR is in the fine tune mode, the trajectory tracking of line segments is illustrated in Fig. 8. To begin with, the turning angle δ_{i-1} of the *(i-1)th* segment is defined as the relative angle between the *ith* segment and the *(i-1)th* segment. The turning point p_{i-1} or turning length l_{i-1} of the *(i-1)th* segment in Fig. 8 is represented as the point or the position, starting to turn into the *ith*

segment. Finally, the following relation $l_{i-1} = c_2(\delta_{i-1})^{c_1}$, where $c_1 = 0.6$, $c_2 = 41.5cm$, and the unit of δ_{i-1} is radian, is employed to track a trajectory of line segments.

C. Strategy of obstacle avoidance

It is assumed that the dimension of the obstacle is not too large to hind the sight of CCD cameras. When a CLMR is in the face of static and dynamic obstacles, the strategy can be simultaneously applied to avoid these obstacles. The strategy for the avoidance of static obstacle in Fig. 9 is first described as follows. (i) As the distance between the corresponding point of the CLMR and the obstacle is smaller than $L_{1,\min}$, the CLMR starts to avoid the corresponding obstacle. That is, the operation of the CLMR is in a mode of static obstacle avoidance. It is not limited to one static obstacle. (ii) As the minimum distance between the corresponding point of the CLMR and the obstacle is greater than $L_{2,\min}$, then $\theta_{1d} = 0$ so that the CLMR moves in a straight line. The minimum distance of the front and back sections is set to zero so that the CLMR is in the mode of static obstacle avoidance. (iii)As $|\alpha - \beta| > 90^\circ$, the operation of the CLMR returns to the trajectory tracking mode.

Similarly, the strategy for the avoidance of dynamic obstacle in Fig. 10 is depicted as follows. (i) As the value $\bar{y}$ of the CLMR is smaller than $y_{\min}$, the CLMR stops.(ii)The CLMR starts to track the trajectory when either of the following conditions is satisfied. (a) $\bar{x} > x_{depature}$, where $\bar{x}$ is the distance between the intersection of trajectory and the center of the CLMR, departing the intersection, and $x_{depature}$ is an assigned distance to prevent the CLMR from bumping against dynamic obstacle. (b) $\tilde{x} > x_{arrival}$, where $\tilde{x}$ is the distance between the intersection of trajectory and the center of the CLMR, arriving the intersection, and $x_{arrival}$ is an assigned distance to prevent the CLMR from bumping against dynamic obstacle.

4.2 Experimental Results

First, the parameters for the obstacle avoidance are $L_{1,\min} = 55$, $L_{2,\min} = 10$, $x_{departure} = 20$, $x_{arrival} = 60$, $y_{\min} = 60cm$, and $\gamma = 60^\circ$. The positions of two static obstacles with radius $7cm$ are $(-70.5, 251.4)$ and $(84.8, 264.5)cm$. The path to be tracked is made up by five segments of straight line (i.e., the dash line in Fig. 11). The sampling time of this paper is $300ms$. The scaling factors $G_s = G_2$, $G_{\dot{s}} = diag\{50, 300\}$, and $G_3 = 6I_2$ are selected. Similarly, the coefficients for the sliding surface are set as $G_1 = diag\{3125, 300\}$ and $G_2 = diag\{12.5, 1.2\}$, which possess a larger value in the 2nd subsystem as compared with the unloaded CLMR (i.e., it does not the contact with ground). Then the responses of four specific cases are shown in Fig. 11. The appropriate parameters of PID control are selected from the responses of the unloaded CLMR as compared with the proposed control. These responses for the unloaded CLMR by PID control and the proposed control are all in acceptable manner. Based on this constraint, their responses in the loaded cases (i.e., Figs. 11(a)-(f) for the FDVSC and Figs. 11(g) and (h) for the PID control) are compared. Although the line segments to be tracked are in the periphery of intelligent space, possessing poor quality for pose estimation, the acceptable performances in Figs. 11(a)-(f) validate the usefulness of our control system.

V. CONCLUSIONS

In a network-based intelligent space of this paper, many problems encountered by classic mobile robots are solved. No mathematical model for the less known CLMR is required for the controller design. First, the values of G_1 and G_2 are chosen to stabilize the sliding surface with appropriate dynamics. The scaling factors G_s and $G_{\dot{s}}$ are employed to normalize the sliding surface and its derivative. Based on the system stability, the output scaling factor G_3 is selected. Although the discontinuity and poor quality of image system in the vicinity of the overlap region exist, its performance is acceptable. Although a minimum turning radius for a CLMR exists, the tracking performance for the line segment with large turning angle is also satisfactory. If the monitoring region is larger, the number of the CCD cameras should be increased or active CCD cameras should be considered.

REFERENCES

[1] F. Zhao and L. Guibas, *Wireless Sensor Networks: An Information Processing Approach*, Elsevier Inc., 2005.

[2] S. Se, D. G. Lowe and J. J. Little, "Vision-based global localization and mapping for mobile robots," *IEEE Trans. Robot. & Automat.*, vol. 21, no. 3, pp. 364-375, Jun. 2005.

[3] S. X. Yang and Q. H. Meng, "Real-time collision-free motion planning of a mobile robot using a neural dynamics-based approach," *IEEE Trans. Neural Networks*, vol. 14, no. 6, pp. 1541-1552, Nov. 2003.

[4] T. H. S. Li, S. J. Chang, "Fuzzy target tracking control of autonomous mobile robots by using infrared sensors," *IEEE Trans. Fuzzy Syst.,* vol. 12, no. 4, pp. 491-501, Aug. 2004.

[5] C. L. Hwang, L. J. Chang and Y. S. Yu, "Network-based fuzzy decentralized sliding-mode control for car-like mobile robots," *IEEE Trans. Ind. Electron.*, vol. 54, no. 1, pp. 574-585, Feb. 2007.

[6] P. L. Tang and C. W. de Silva, "Compensation for transmission delays in an Ethernet-based control network using variable-horizontal predictive control," *IEEE Trans. Contr. Syst. Technol.*, vol. 14, no. 4, pp. 707-718, Jul. 2006.

[7] W. J. Kim, K. Ji, and A. Ambike, "Real-time operating environment for networked control systems", *IEEE Trans. Automat. Sci. & Engrg.*, vol. 3, no. 3, pp. 287-296, Jun. 2006.

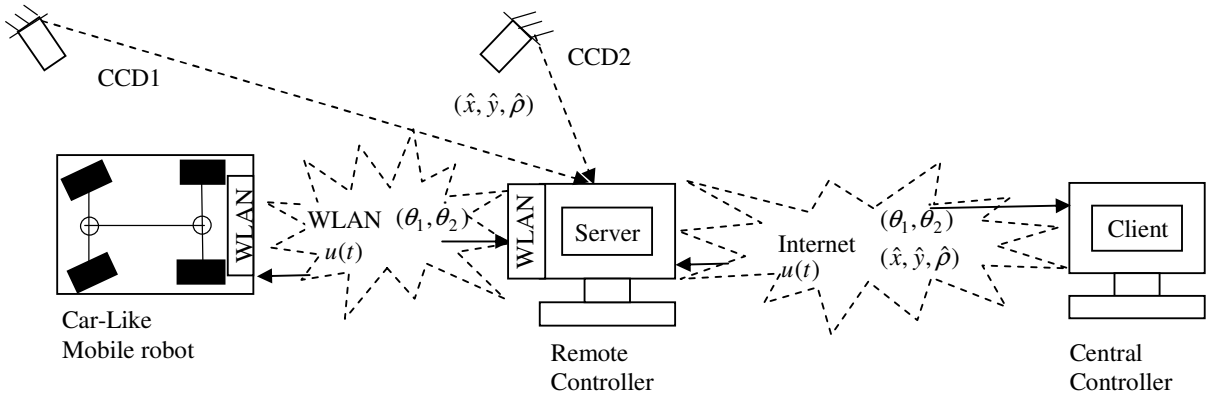

Fig. 1. Block diagram of the overall system.

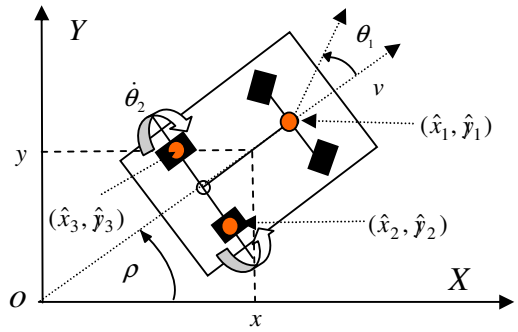

Fig. 2. Kinematics and three positions of LED for the CLMR.

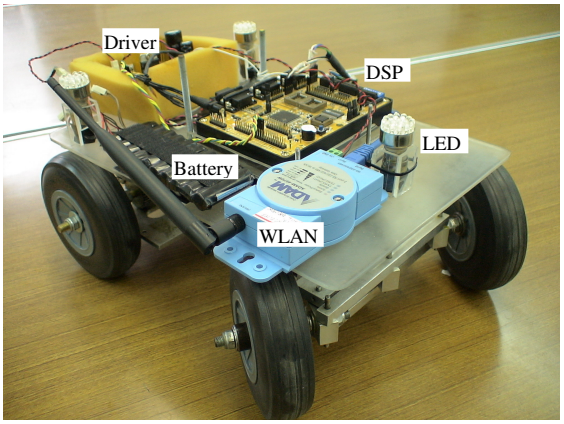

Fig. 3. Implementation of the CLMR.

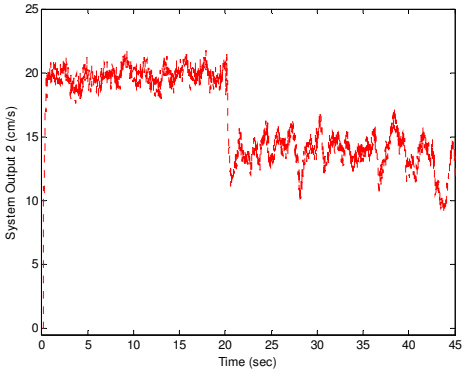

(a)The response of rear-wheel for two step inputs $v_d = 20.4cm/s$ at $t = 0s$ and $\theta_{1d} = 30°$ at $t = 20s(\cdots)$;

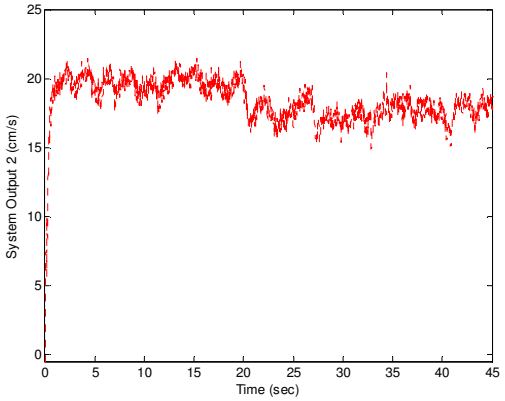

(b) The response of rear-wheel for two step inputs $v_d = 20.4cm/s$ at $t = 0s$ and $\theta_{1d} = 15°$ at $t = 20s(\cdots)$;

Fig. 4. Step responses of CLMR.

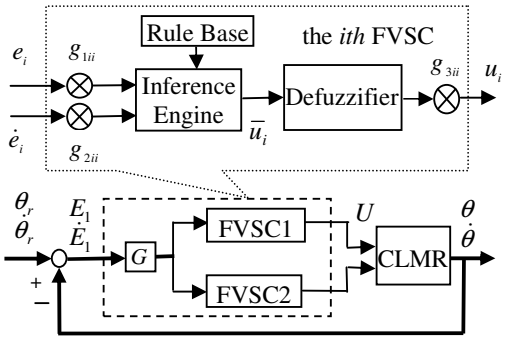

Fig. 5. Block diagram of FDVSC.

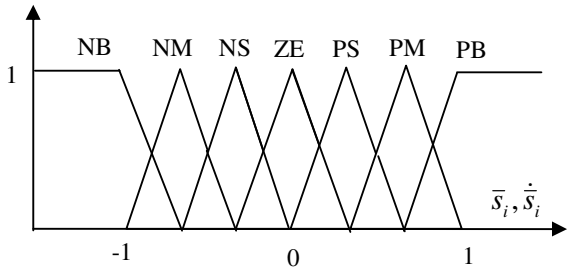

Fig. 6. Membership functions with triangular type.

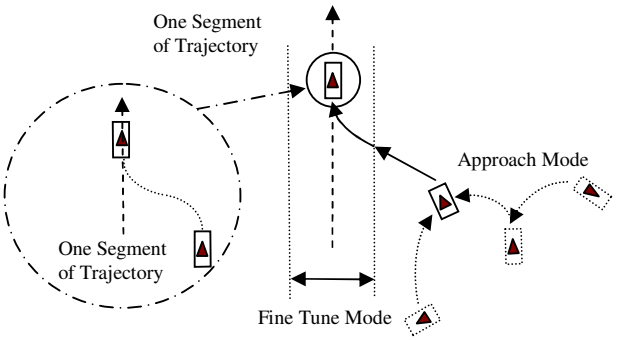

Fig. 7. Illustration of trajectory tracking mode.

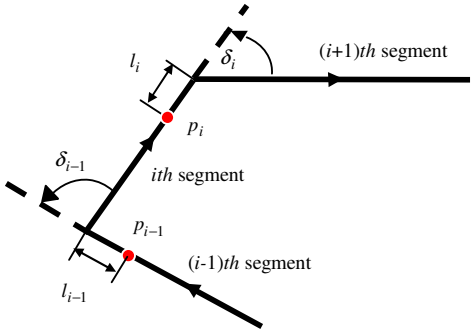

Fig. 8. Illustration of trajectory tracking of line segments.

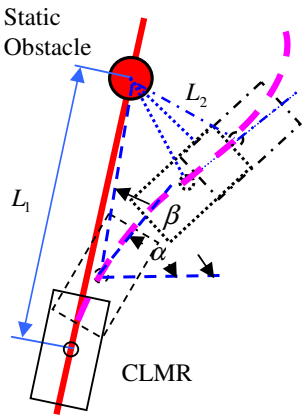

Fig. 9. The strategy for the avoidance of static obstacle.

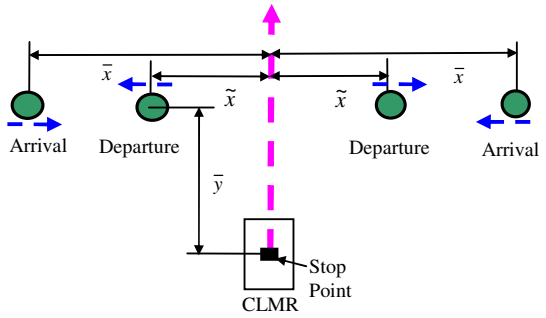

Fig. 10. The strategy of avoidance of dynamic obstacle.

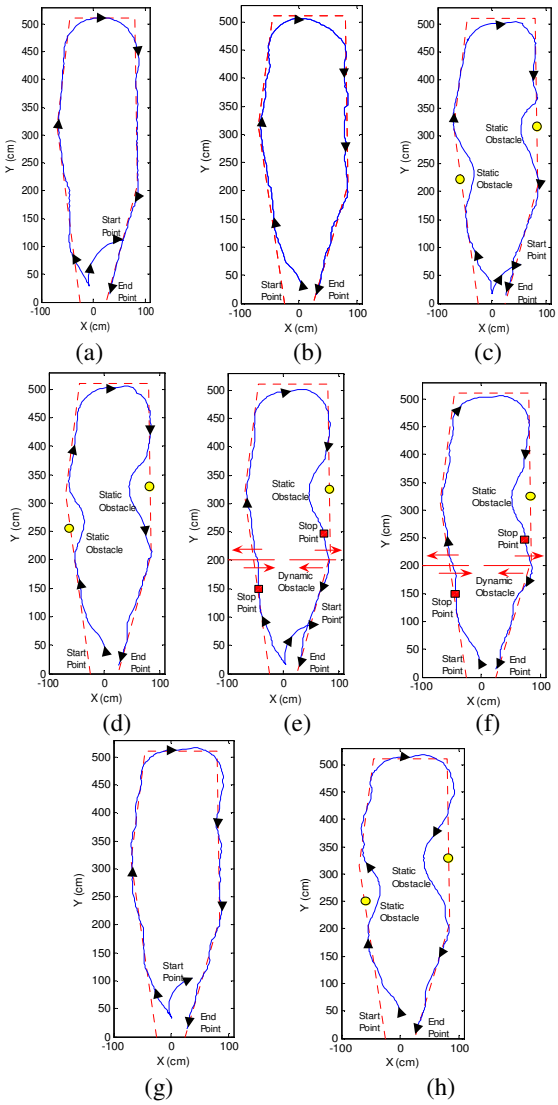

Fig. 11. Responses of the trajectory tracking of the CLMR in the network-based intelligent space for the following four cases: (a) and (b), the proposed control without obstacle; (c) and (d), the proposed control with two static obstacles; (e) and (f), the proposed control with one static obstacle and one dynamic obstacle; (g), PID control without obstacle; (h), PID control with two static obstacles.

Table 1. Rule table of the *ith* FDVSC.

$\bar{S}_i$ \ $\dot{\bar{S}}_i$	PB	PM	PS	ZE	NS	NM	NB
NB	ZE	NS	NM	NB	NB	NB	NB
NM	PS	ZE	NS	NM	NB	NB	NB
NS	PM	PS	ZE	NS	NM	NB	NB
ZE	PB	PM	PS	ZE	NS	NM	NB
PS	PB	PB	PM	PS	ZE	NS	NM
PM	PB	PB	PB	PM	PS	ZE	NS
PB	PB	PB	PB	PB	PM	PS	ZE